Received: 2 August 2023 | Revised: 25 January 2024 | Accepted: 28 January 2024
DOI: 10.1002/jrs.6663

RESEARCH ARTICLE

Journal of RAMAN SPECTROSCOPY WILEY

High-pressure and high-temperature Raman spectroscopic study of zircon as a pressure scale in hydrothermal DACs

Naoko Takahashi | **Hiroki Kobayashi** | **Hiroyuki Kagi**

Geochemical Research Center, Graduate School of Science, The University of Tokyo, Tokyo, Japan

Correspondence
Naoko Takahashi, Geochemical Research Center, Graduate School of Science, The University of Tokyo, 7-3-1 Hongo, Bunkyo-ku, Tokyo 113-0033, Japan.
Email: ntakahashi@eqchem.s.u-tokyo.ac.jp

Funding information
JSPS KAKENHI Grant/Award Number: JP22J00992.

Abstract

Raman spectra of zircon have recently been used as a pressure scale for studies of geological fluids at high temperatures and high pressures using diamond anvil cells (DACs). The zircon scale is advantageous in high chemical stability and the large pressure response of the B_{1g} mode. Despite its excellent applicability, the calibration of the scale has been carried out only in a narrow pressure–temperature range, especially under limited high-temperature and high-pressure conditions. In this study, the pressure and temperature dependence of the Raman modes of synthetic zircon was investigated up to 9.5 GPa and from room temperature to 776 K using an externally heated diamond anvil cell. Ruby and gold were used as the reference pressure scales. The Raman shift of the B_{1g} mode for the antisymmetric stretching of the SiO_4 structure in zircon showed a linear pressure dependence of 5.48(4) cm^{-1}/GPa up to 8 GPa at room temperature, in agreement with the previous studies. Measurements under high-pressure and high-temperature conditions confirmed that the pressure dependence up to 9.5 GPa along the isotherms from 373 to 675 K was consistent with the room-temperature value; the wavenumbers can be well deduced from the sum of the individual effects of pressure and temperature, obtained at ambient temperature and pressure, respectively. A comparison of the zircon scale with the *c*-BN Raman spectroscopic scale confirmed that the pressures determined with these scales were in reasonable agreement. The present results provide a confident use of the zircon Raman spectroscopic scale in a wider pressure–temperature range than previous studies for the internally consistent pressure determination.

KEYWORDS
diamond anvil cell, optical pressure scale, Raman spectroscopy, X-ray diffraction, zircon

1 | INTRODUCTION

High-pressure experiments are essential to elucidate the behavior of materials in the Earth's and planetary interiors. Pressure in a sample chamber of a high-pressure device, such as a diamond anvil cell (DAC), is often estimated using a pressure scale loaded together with the samples. Appropriate pressure scales should be selected for each experiment to meet the experimental requirements, for example, desired precision and accuracy, chemical inertness, and stability in the pressure–temperature region of interest. Equations of state (EoS) of some elemental metals and simple compounds such as MgO provide the most accurate pressure estimation as they are called primary pressure scales. These EoS have been derived from dynamic shock wave experiments[1] or from combined measurements of density by X-ray diffraction (XRD) and acoustic wave velocities by Brillouin scattering.[2] However, primary scales are not always available or suitable depending on the experimental instrumentation and conditions. For example, some high-pressure devices are not capable of in situ diffraction measurements, which prevents access to the unit-cell volume of a primary scale. In such cases, optical spectroscopy-based pressure scales calibrated with other scales are alternative ways to estimate pressure. The most commonly used ruby scale[3,4] (see the review by Syassen[5]) is advantageous in the high intensity of the *R*1 fluorescence line, the large wavelength shift to pressure, and the stability up to megabars. However, this scale is unsuitable for high-temperature experiments because its linewidth broadens and its intensity decreases with increasing temperature.[6] Other fluorescence pressure scales, such as Sm-doped strontium borate ($SrB_4O_7{:}Sm^{2+}$)[7–11] and Sm-doped yttrium aluminum garnet ($Y_3Al_5O_{12}{:}Sm^{3+}$),[12–16] have also been proposed, offering accurate pressure determination at high temperatures owing to the very small temperature dependence of the fluorescence lines. However, these fluorescence scales react with corrosive media such as H_2O at high temperatures, which limits their application under such experimental conditions.[17,18]

Various optical pressure scales based on Raman spectroscopy have been established, including α-quartz,[19] ^{13}C diamond,[18,20–22] cubic boron nitride (*c*-BN),[23–29] berlinite ($AlPO_4$),[30] cubic silicon carbide (3C-SiC),[31] zircon,[32] and carbonate minerals.[33] Owing to the high chemical resistance to many solids and liquids at high temperatures, ^{13}C diamond, *c*-BN, and zircon have been recognized as good scales in studies of deep geological fluids using hydrothermal DACs (see the review by Schmidt and Chou[34]). Since the first calibration by Schmidt et al.,[32] the zircon scale has been commonly used because (1) zircon is chemically resistant to aqueous fluids[35,36] and hydrous silicate melts[37]; (2) zircon is widely available and can be easily synthesized in millimeter sizes[38,39]; and (3) the antisymmetric vibrations of the SiO_4 structures in zircon show a linear pressure-induced shift of 5.8 ± 0.1 cm^{-1}/GPa,[32] which is larger than the that of the longitudinal transverse optical (LTO) mode of ^{13}C diamond (2.8 cm^{-1}/GPa)[18,20] and the transverse optical (TO) mode of *c*-BN (3.4 cm^{-1}/GPa).[23]

Zircon ($ZrSiO_4$) has a tetragonal crystal structure with the space group $I4_1/amd$, consisting of a chain of alternating edge-sharing SiO_4 tetrahedra and ZrO_8 triangular dodecahedra. According to previous experimental[40] and theoretical[41] studies, zircon transforms into reidite at pressures of 8–10 GPa at 1100–1900 K and around 9 GPa at 0 K, respectively. The Raman-active vibrational modes of zircon include the A_{1g}, B_{1g}, B_{2g}, and E_g symmetries and can be divided into three vibrational groups: internal SiO_4 vibrations, external vibrations involving lattice vibrations of the SiO_4 group as a unit and Zr cations, and their mixture.[42–44] The modes A_{1g} around 439 and 975 cm^{-1} and B_{1g} around 1008 cm^{-1} are generally assigned to internal SiO_4 bending, symmetric stretching, and antisymmetric stretching, respectively.[42–45] There remains disagreement about the assignment of the low-wavenumber vibrational modes. The mode E_g around 201 cm^{-1} is interpreted as an external translational[42,43,45] or rotational mode.[44,46] The mode E_g around 224 cm^{-1} is interpreted as an external rotational,[42,43] translational,[44] or mixed vibration.[45] The E_g mode around 356 cm^{-1} was interpreted as an external rotational[43–46] or internal antisymmetric bending vibration.[42] The temperature dependence of the wavenumbers of zircon Raman modes at ambient pressure was recorded at 90 and 295 K[43] and at temperatures at 295–1273 K[32] and 80–1400 K.[47] The pressure dependence at room temperature has been experimentally well investigated on synthetic zircon[32,48] and natural non-metamict or metamict zircon[48–50] using the ruby fluorescence scale as a reference. Schmidt et al.[32] further studied simultaneous high-pressure and high-temperature effects on the B_{1g} mode around 1008 cm^{-1} up to 973 K and 1.2 GPa based on the constant volume approach using the EoS of H_2O[49] and established a pressure scale using the B_{1g} mode of zircon for hydrothermal DAC experiments. However, the pressure dependence of the Raman spectra of zircon at high temperatures has not yet been studied above 1.2 GPa, and the empirical calibration equations are not validated beyond the calibration conditions.

To establish a reliable zircon pressure scale for application in a wider range of temperature–pressure conditions, we investigated the pressure and temperature dependence of Raman modes of zircon up to 9.5 GPa and 776 K, against reference pressure standards of ruby and gold, which were presented as internally consistent scales.[51,52] We also compared the performance of zircon and *c*-BN as Raman spectroscopic pressure scales at high temperatures and high pressures. This study would contribute to constructing a database with internally consistent pressures as well as a better understanding of the pressure and temperature-dependent evolution of the vibrational properties of zircon.

2 | EXPERIMENTAL METHODS

We conducted four kinds of experiments: (1) compression experiment at room temperature, (2) heating experiment at ambient pressure, (3) high-pressure and high-temperature experiments, and (4) case study: comparison with the *c*-BN scale. Single crystals of about 10 μm in size obtained by crushing zircon pieces synthesized using a Li–Mo flux technique were used as a starting material. All experiments were performed using an externally heated hydrothermal diamond anvil cell (Bassett-type HDAC-V[53,54]) equipped with type-Ia diamond anvils with a culet diameter of 300 or 600 μm. Temperature was measured using two K-type thermocouples cemented to the upper and lower anvils. The thermocouple was calibrated using the melting temperatures of native sulfur (99.999% purity, Strem Chemicals, Inc.; 386.0 K) and sodium chloride (FUJIFILM Wako Pure Chemical Corp.; 1074 K). These substances in the sample chamber were placed at the center of the anvil. The thermocouple readings were 0.2 K lower than the melting temperature of native sulfur and 5 K lower than that of sodium chloride. To calibrate the thermocouple temperatures, a linear equation was derived based on the differences between the measured temperatures and the known melting temperatures. The temperature fluctuations during XRD and Raman measurements were below ±1 K. Above 473 K, a mixture of Ar + 2% H_2 gas was flowed into the gas chamber to prevent oxidation of the Mo heating wires and tungsten carbide cores. Iridium or rhenium gaskets were used to load samples and a pressure-transmitting media (PTM). For the high-pressure experiments, the gaskets with an initial thickness of 125 μm were pre-indented to ~8 GPa and then drilled a hole with a diameter of 150 μm for a sample chamber. Details of each experimental method are given below.

2.1 | Room-temperature compression experiment

Room-temperature compression experiment was performed up to 8 GPa using a 4:1 methanol–ethanol mixture PTM that remains hydrostatic up to approximately 10 GPa.[55–57] A piece of zircon, the PTM, and a ruby sphere as a pressure standard were loaded into the sample chamber. Raman spectra of zircon and fluorescence spectra of ruby were collected at the synchrotron beamline BL-18C in the Photon Factory, High-Energy Accelerator Research Organization (KEK), using an imaging spectrometer equipped with a grating of 1800 lines/mm (Princeton Instruments, Acton standard series SP-2750 imaging spectrograph) coupled to an electron-multiplying charge-coupled devices (EMCCD) camera with an imaging array of 1600 × 200 pixels (Princeton Instruments, ProEM eXcelon3) in backscattering geometry. A diode-pumped solid-state (DPSS) 532-nm laser (Gem 532, Laser Quantum) was used for excitation. The laser power measured at the focal point with a long working distance objective lens (Mitutoyo, M Plan Apo 20×, N.A. = 0.42) was ~15 mW. For ruby fluorescence measurements, the laser power was reduced to 0.1% by inserting a neutral density filter. Ruby fluorescence spectra and Raman spectra of zircon were obtained with three accumulations for a 0.1-s exposure time and 20 to 30 accumulations for a 20-s exposure time, respectively. The reference wavelength of ruby *R*1 fluorescence at ambient pressure was monitored in each pressure measurement by measuring a ruby sphere placed on the table of the anvil. Raman spectra of zircon were recorded in two wavenumber regions (~10–880 cm^{-1} and ~320–1160 cm^{-1}), because not all the Raman-active modes were covered in a single spectral window. Raman spectra of 4-acetamidophenol were also collected in each run for wavenumber calibration. The Raman shift was calibrated with quadratic and linear functions using peaks of a 4-acetamidophenol[58] at 213.3, 329.2, 390.9, and 465.1 cm^{-1} for the low-wavenumber regions and 968.7 and 1105.5 cm^{-1} for the high-wavenumber region, respectively. After the calibration, the Raman modes of zircon at ambient conditions were centered at 200.7, 213.1, 223.8, 355.9, 438.7, 974.2, and 1007.9 cm^{-1}, which are well consistent with the room-temperature data from Schmidt et al.[32] Peak positions were determined using PeakFit v4.12 software; Voigt and Gaussian–Lorentzian area functions were respectively used to fit ruby fluorescence and Raman spectra, where the background intensities were subtracted using cubic functions. In general, curve fitting notably improves the precision in determining peak position.[59] The wavenumber precision of the intense B_{1g} mode after curve fitting was less than 0.08 cm^{-1}, although the wavenumber dispersion of the spectrometer is about 0.5 cm^{-1}/pixel. Nonetheless, we monitored the peak position of the neon line over several hours during the experiments, which was found to yield a standard deviation of 0.2 cm^{-1}. We therefore consider

±0.2 $\mathrm{cm^{-1}}$ to be the random error of the Raman spectroscopic measurements. Pressures were calculated using the calibration curves of the ruby $R1$ fluorescence of Piermarini et al.[60] and Dorogokupets and Oganov.[51] The precision of the pressure determined by the ruby fluorescence was assumed to be ±0.05 GPa.

2.2 | Ambient-pressure heating experiment

Ambient-pressure heating experiment was performed up to 1078 K to check the reproducibility of previously reported results. Raman spectra of zircon were obtained using an in-house experimental setup at the University of Tokyo, an imaging spectrograph equipped with a grating of 1200 lines/mm (Chromex, 500is), coupled with a charge-coupled device (CCD) camera with 1024 × 128 pixels (Andor Technology, DU401A BR-DD) in backscattering geometry. A 514.5-nm $\mathrm{Ar^+}$ laser (Modu-Laser) was used for excitation, where the laser power at the focal point with a long working distance objective lens (Olympus, SLMPlan 20×, N.A. = 0.35) was ~3 mW. Each Raman spectrum of zircon was obtained by accumulating 30 exposures for 10 s in a single wavenumber region (~70–1570 $\mathrm{cm^{-1}}$). The calibration of the Raman shift using a 4-acetamidophenol and the data analysis were the same as described in Section 2.1. Although the wavenumber dispersion of the spectrometer is about 1.5 $\mathrm{cm^{-1}}$/pixel, the wavenumber precision of the intense B_{1g} mode after curve fitting was improved to less than 0.04 $\mathrm{cm^{-1}}$.

2.3 | High-pressure and high-temperature experiments

High-pressure and high-temperature experiments were performed in the range of 373–776 K and 0.6–9.5 GPa using purified H_2O (Milli-Q water) as the PTM. In addition to a piece of zircon and the PTM, gold powder (99.5% purity, Nilaco Corp.) as a pressure standard was loaded into the sample chamber. The samples were first compressed at room temperature and then heated, and data were collected along heating or cooling paths. In situ Raman spectra of zircon and powder XRD data were collected at synchrotron beamline BL-18C in the Photon Factory, KEK. Synchrotron X-rays were monochromatized by a double crystal Si(111) monochromator ($\lambda = 0.619$ Å) and collimated to 60 μm. XRD patterns were collected for 1 min using a Flat Panel detector (Rad-icon 2022) in a Debye–Scherrer geometry. The X-ray wavelength and the detector distance were calibrated using the NIST CeO_2 standard using IPAnalyzer software.[61] The two-dimensional XRD patterns were converted into one-dimensional profiles using the IPAnalyzer software.[59] The unit-cell volume of gold was determined by fitting the 111 and 200 reflections in the Le Bail method using the GSAS-EXPGUI software.[62,63] In some cases, gasket materials (rhenium or indium) and/or solidified PTM (H_2O ice VII) were also included in the Le Bail fitting for better results. The representative fitting results are shown in Figure S1. The pressure was determined using an EoS of gold given by Dorogokupets and Dewaele.[52] The experimental setup for in situ Raman spectroscopy and the data analysis were the same as described in Section 2.1.

2.4 | Case study: comparison with the *c*-BN scale

In addition to the calibration experiments, a case study was conducted to compare the pressures determined with the zircon and *c*-BN pressure scales. A piece of zircon, *c*-BN (Global Diamond Co., Ltd.), and alkaline silica solution (Na/Si = 1) prepared with silica gel (MP Biomedicals Inc.) and 1-mol/L sodium hydroxide solution (FUJIFILM Wako Pure Chemical Corp.) were loaded into the sample chamber. Raman spectra of zircon and *c*-BN were obtained at an in-house experimental setup in the University of Tokyo as described in Section 2.2. Each Raman spectrum of zircon was obtained by accumulating 30 exposures for 10 s in a single wavenumber region (~70–1570 $\mathrm{cm^{-1}}$) and was processed in the same way as described in Section 2.1.

3 | RESULTS AND DISCUSSION

3.1 | Room-temperature compression experiment

Figure 1 and Table S1 show the pressure dependence of the observed Raman modes of zircon up to 8 GPa at room temperature. All the Raman modes show an increase in wavenumber with pressure, except for the E_g, ω_{201} mode. The mode wavenumber $\omega_{i,P}$ at a pressure P can be described by a linear equation:

$$\omega_{i,P} = bP + \omega_{i,\ 0.1\,MPa} \tag{1}$$

where b is a linear pressure coefficient ($\partial\omega_i/\partial P$) and $\omega_{i,\ 0.1\,\mathrm{MPa}}$ is the wavenumber at ambient pressure. A bivariate weighted fit method[64] with the implemented code[65] was used for estimating the best fit to account for the uncertainties in the individual data points. The uncertainties in $\omega_{i,P}$ reflect the total propagated errors from the standard errors of the peak fitting results and the random errors assumed to be ±0.2 cm^{-1}. The uncertainties in P were assumed to be ±0.05 GPa. Table 1 and Table S2 respectively show the resulting parameters of the B_{1g} mode and other modes using the calibration curves of ruby $R1$ fluorescence of Piermarini et al.[60] and Dorogokupets and Oganov[51] for pressure determination. We compared our results with previous experimental data of Schmidt et al.[32] up to 6.6 GPa and Pina Binvignat et al.[50] up to 9.3 GPa and found overall good agreement with the trends, especially with the linear regression coefficients of Pina Binvignat et al.[50] The pressure shifts for the E_g, ω_{224} mode deviates slightly from those reported in the previous study[32] as the peak overlaps with B_{1g} mode around 215 cm^{-1} at high pressures. In the case of E_g, ω_{356} mode, there appears to be a discrepancy between our data and those obtained by the previous study,[32] even after accounting for the uncertainty in the regression coefficients. The linear pressure coefficient for the B_{1g}, ω_{1008} mode up to 8 GPa with the ruby fluorescence method by Piermarini et al.[60] is well consistent with the data of Schmidt et al.[32] using the same calibration curve, within 3σ uncertainties (Table 1). For optimizing a zircon pressure scale (Section 3.4), we use the calibration of ruby fluorescence by Dorogokupets and Oganov,[51] because it was presented as an internally consistent scale with gold.

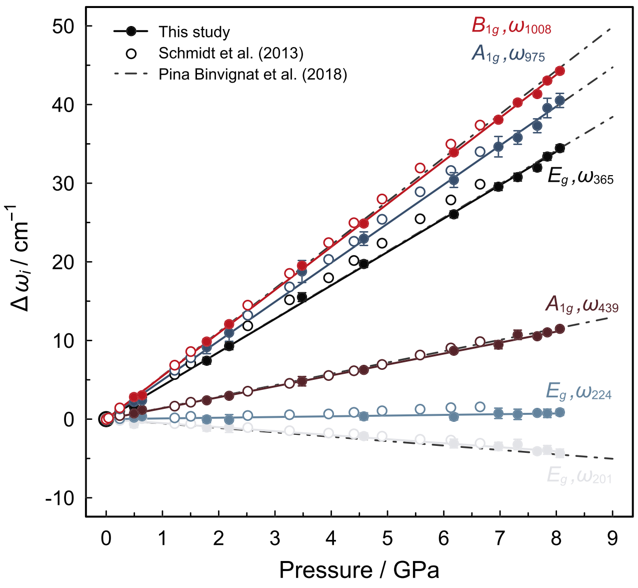

FIGURE 1 Pressure dependences of the wavenumber for the Raman modes of zircon at room temperature. $\Delta\omega_i$ is defined as $\Delta\omega_i = \omega_i - \omega_{i,\,0.1\ \mathrm{MPa}}$ where ω_i is the observed wavenumber under pressure and $\omega_{i,\,0.1\ \mathrm{MPa}}$ is the wavenumber at ambient pressure calculated from a linear regression. The present data (filled circle) are consistent with previous studies (open circle, Schmidt et al.[32]; dashed line, Pina Binvignat et al.[48]).

3.2 | Ambient-pressure heating experiment

Figure 2 shows the temperature dependence of the observed Raman modes of zircon at ambient pressure. All the Raman modes showed a nonlinear decrease in wavenumber with temperature. The temperature dependence of the wavenumber for the Raman modes of zircon was previously investigated by Schmidt et al.[32] from 295 to 1223 K and Stangarone et al.[47] from 80 to 1400 K at ambient pressure. Our data at ambient pressure measured from 294 to 1078 K well reproduced the results reported by Schmidt et al.[32] (Figure 2). The discrepancy with Stangarone et al.[47] increases with increasing temperature, reaching 2 cm^{-1} at 1073 K for the B_{1g}, ω_{1008} mode. The data of the B_{1g} mode from 295 to 1223 K obtained by Schmidt et al.[32] were used for the zircon pressure scale (Section 3.4).

Stangarone et al.[47] demonstrated that phonon-mode Grüneisen tensor coefficients of zircon Raman modes, calculated using Hartree-Fock/Density Functional Theory simulations, successfully reproduced the experimentally observed wavenumber changes with pressure at

TABLE 1 Linear pressure coefficients, wavenumbers at zero pressure for the B_{1g}, ω_{1008} mode of zircon, obtained from the room-temperature compression data.

References	P_{max} (GPa)[a]	$\partial\omega_{1008}/\partial P$ (cm^{-1}/GPa)[b]	$\omega_{1008,\ 0.1\ \mathrm{MPa}}$ (cm^{-1})[b]
Schmidt et al.[32]	6.6	5.69(2)	1007.9(1)
Pina Binvignat et al.[47]	9.3	5.54(5)	1008.6(3)
This study (P_{R1}: P75)	8.0	5.56(4)	1008.4(2)
This study (P_{R1}: DO07)	8.1	5.48(4)	1008.6(2)

[a] Maximum pressure of the experimental data.

[b] $\partial\omega_{1008}/\partial P$ and $\omega_{1008,\ 0.1\ \mathrm{MPa}}$ were calculated with normal linear regression in the previous studies and bivariate linear weighted regression in this study. Pressures were calculated using the calibration curves of ruby fluorescence $R1$ line of Piermarini et al.[60] (P75) and Dorogokupets and Oganov[51] (DO07).

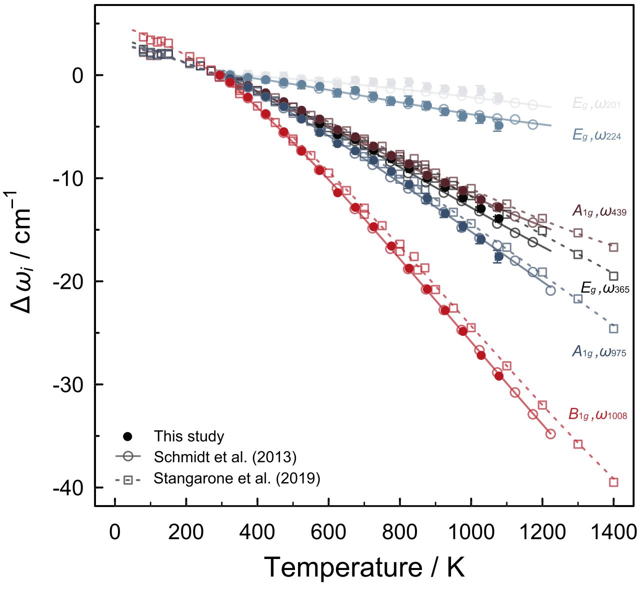

FIGURE 2 Temperature dependences of the wavenumber for the Raman modes of zircon at ambient pressure. $\Delta\omega_i$ is defined as $\Delta\omega_i = \omega_{i,} - \omega_{i,\,\mathrm{RT}}$ where ω_i is the observed wavenumber at high temperatures and $\omega_{i,\,\mathrm{RT}}$ is the observed wavenumber at room temperature. The present data (filled circle) are well consistent with the data of Schmidt et al.[32]).

room temperature. However, these coefficients cannot reproduce the experimentally observed wavenumber changes with temperature at ambient pressure. This along with the band broadening of all the observed Raman modes of zircon with temperature[32] suggests that there are important contributions from explicit anharmonicity due to phonon–phonon interactions. Here, the temperature dependence is further divided into two terms: (1) the implicit quasiharmonic contribution, reflecting the effect of the change in equilibrium interatomic spacings due to lattice thermal expansion, that is, attributable simply to the volume change with temperature, and (2) the explicit contribution of anharmonicity, reflecting the effect of the change in vibrational amplitudes at fixed equilibrium positions, that is, the pure temperature effect at constant volume.[66] The general mathematical expression is as follows:

$$\left(\frac{\partial \ln\omega_i}{\partial T}\right)_P = -\frac{\beta}{\kappa}\left(\frac{\partial \ln\omega_i}{\partial P}\right)_T + \left(\frac{\partial \ln\omega_i}{\partial T}\right)_V \tag{2}$$

$$= -\beta\gamma_{iT} + \left(\frac{\partial \ln\omega_i}{\partial T}\right)_V \tag{3}$$

where β and κ are the volume thermal expansion coefficient and the isothermal volume compressibility, respectively. The term on the left-hand side gives the observed temperature-dependent change in the mode wavenumbers, whereas, on the right-hand side, the first term is the implicit contribution and the second term is the explicit contribution. Equation (3) is derived by defining the relative change of the mode wavenumbers to the relative change of volume, corresponding to an isothermal mode Grüneisen parameter $\gamma_{iT} = -\kappa^{-1}(\partial \ln\omega_i/\partial P)$. The γ_{iT} is nearly independent of temperature and thus assumed to be constant. Indeed, the pressure dependence of the Raman modes, at least the B_{1g}, ω_{1008} mode, was nearly constant up to 776 K, as shown in the next section. Table S3 reports the anharmonicity parameters calculated using the logarithmic isobaric temperature derivatives and the isothermal pressure derivatives of wavenumbers, and the isothermal volume compressibility and the thermal expansion coefficient from the isothermal-type EoS of zircon.[67] We find that the explicit anharmonicity equals or dominates the implicit contribution and largely contributes to the observed temperature-induced shifts for all the external and internal modes. Note that the decreased temperature derivatives of the modes at low temperatures[47] decrease the contribution of the anharmonicity term. The A_{1g}, ω_{439} mode that is related to internal SiO_4 bending[42–45] shows the most pronounced anharmonicity, which is consistent with the significant broadening of the mode with increasing temperature as shown in Figure S2. The largest softening of the E_g, ω_{356} mode (Figure S2) is owing to high values of both implicit contribution and explicit anharmonicity, which implies that this external rotational vibration[43–46] strongly responds to changes in volume and temperature.

3.3 | High-pressure and high-temperature experiments

A series of high-pressure and high-temperature experiments was carried out at temperatures up to 776 K and pressures up to 9.5 GPa to check the absence of temperature dependence of the pressure-induced shifts of Raman modes of zircon. Figure S3 shows the pressure- and temperature-dependent wavenumbers of four Raman modes with enough intensity for extracting wavenumber information. The E_g, ω_{356} mode and A_{1g}, ω_{439} and ω_{975} modes showed linear trends along each isotherm but are relatively scattered, especially for the A_{1g}, ω_{439} mode. The excellent linear correlation along each isotherm was observed for the B_{1g}, ω_{1008} mode with the high intensity and the large pressure response. Table 2 summarizes the pressure and temperature-dependent B_{1g} mode wavenumber. The bivariate weighted fit method was used to find the slope and the associated standard error in a relation between the pressure given by the unit-cell volume

TABLE 2 Pressure and temperature-dependent B_{1g}, ω_{1008} mode wavenumber of zircon and the pressures calculated with Equation (6).

T (K)	P_{Au} (GPa)[a]	B_{1g}, ω_{1008} (cm^{-1})[b]	P_{calc} (GPa)[c]
373	1.14(1)	1012.04(2)	1.1(1)
373	1.69(1)	1015.56(3)	1.8(1)
373	2.08(1)	1016.57(5)	2.0(1)
373	2.95(1)	1022.45(7)	3.0(1)
373	3.70(1)	1027.67(1)	4.0(1)
373	3.78(2)	1026.76(1)	3.8(1)
373	7.81(1)	1049.37(3)	7.9(1)
373	9.53(2)	1057.43(2)	9.4(1)
474	1.49(1)	1010.93(3)	1.5(2)
474	2.97(1)	1018.55(5)	2.9(2)
474	3.26(1)	1020.88(3)	3.3(2)
474	4.06(1)	1025.24(5)	4.1(2)
474	4.52(2)	1027.33(2)	4.5(2)
474	5.31(1)	1033.59(2)	5.7(2)
474	8.63(1)	1049.07(2)	8.5(2)
474	8.63(2)	1049.29(8)	8.5(2)
575	0.59(1)	1001.67(5)	0.5(2)
575	1.89(2)	1009.51(1)	1.9(2)
575	3.07(1)	1017.5(2)	3.4(2)
575	3.94(1)	1021.0(2)	4.0(2)
575	4.88(1)	1026.27(3)	5.0(2)
575	7.54(2)	1039.51(1)	7.4(2)
575	8.88(1)	1047.74(4)	8.9(2)
675	1.87(1)	1005.63(7)	1.9(2)
675	2.30(2)	1008.45(4)	2.4(3)
675	2.31(1)	1007.42(5)	2.2(3)
675	5.65(1)	1026.66(2)	5.7(3)
675	6.97(1)	1034.4(1)	7.1(3)
726	2.57(1)	1007.87(3)	2.7(3)
776	2.82(2)	1006.92(2)	2.8(3)
776	6.48(1)	1024.87(3)	6.1(3)

[a] P_{Au} represents the pressure estimated from the unit-cell volume of gold. The associated error was calculated by propagating the standard error of the unit-cell volume.

[b] The wavenumber error is derived from the standard error of peak fitting results.

[c] P_{calc} is the pressure calculated by Equation (6) with the observed wavenumber of the B_{1g}, ω_{1008} mode. The corresponding error was calculated by propagating the standard error of the regression parameters and the total error from the standard error of the peak fitting results and the random error.

of gold and the observed wavenumber. The uncertainty in P_{Au} was calculated based on the propagation of the standard error of the unit-cell volume. The uncertainty in ω_{1008} reflects the total propagated errors from the standard errors of the peak fitting results and the random errors of ±0.2 cm^{-1}, as described above in Sections 2.1 and 3.1. The pressure dependences for the B_{1g} mode at each isotherm were 5.46(3) cm^{-1}/GPa to 9.5 GPa at 373 K, 5.37(3) cm^{-1}/GPa to 8.6 GPa at 474 K, 5.45 (3) cm^{-1}/GPa to 8.9 GPa at 575 K, and 5.63(5) cm^{-1}/GPa to 7.0 GPa at 675 K, respectively. These linear pressure coefficients are nearly independent of temperature, giving close agreements within 2σ uncertainties with the value calculated from the data of room-temperature compression experiments using the hydrostatic methanol–ethanol mixture (5.48(4) cm^{-1}/GPa). To check the effect of solidified H_2O on the Raman shift, we calculated the pressure dependence exclusively from data of solidified H_2O regions. The pressure dependence of the B_{1g} mode at 373 K and 3.0–9.5 GPa in H_2O-VII regions was 5.32 (4) cm^{-1}/GPa. This is consistent, within 2σ uncertainties, with the coefficient at 373 K and 1.1–9.5 GPa in liquid-H_2O/H_2O-VII regions (5.46(3) cm^{-1}/GPa), as well as the room-temperature coefficient (5.48(4) cm^{-1}/GPa). Therefore, the shift of the B_{1g} mode is independent of whether the PTM is a solidified or liquid H_2O within the precision of the Raman spectroscopic measurements in this study. Schmidt et al.[32] originally proposed the pressure dependence for the B_{1g} mode of $\partial\omega_{1008}/\partial P = 5.8 \pm 0.1$ cm^{-1}/GPa, which was derived from the room-temperature experiments up to 6.6 GPa and high-temperature and high-pressure experiments up to 973 K and 1.2 GPa. Therefore, we confirmed the negligible temperature dependence of $\partial\omega_{1008}/\partial P$ in a higher pressure range at elevated temperatures than previously reported.

3.4 | Optimization of zircon Raman pressure scale

The empirical equations for pressure and temperature dependence obtained at ambient temperature and pressure, respectively, were tested to be valid for our simultaneous high-pressure and high-temperature data of the Raman shift of B_{1g}, ω_{1008} mode in zircon. For the temperature dependence of the B_{1g} mode of zircon at ambient pressure, we use the rewritten formula of the nonlinear temperature dependence of the B_{1g} mode from 295 to 1223 K reported by Schmidt et al.[32] as follows:

$$\omega_{1008}\left(P_{0.1\,MPa},T\right)=a_0+a_1T+a_2T^2+a_3T^3 \tag{4}$$

where $a_0 = 1015.44(30)$ cm^{-1}, $a_1 = -1.84(14) \times 10^{-2}$ cm^{-1}, $a_2 = -2.23(20) \times 10^{-5}$, $a_3 = 7.54(88) \times 10^{-9}$, and T is temperature in K. The numbers in parentheses represent standard error of the regression coefficients.

The following Equations (5) and (6) are derived by combining Equations (1) and (4).

$$\omega_{1008}(P,T) = a_0 + a_1 T + a_2 T^2 + a_3 T^3 + bP \tag{5}$$

$$P = \frac{\omega_{1008}(P,T) - (a_0 + \mathrm{a}_1 T + a_2 T^2 + a_3 T^3)}{b} \tag{6}$$

Figure 3 shows that these equations explain well the high-pressure and high-temperature experimental data up to 9.5 GPa and 776 K; the wavenumbers can be well deduced from the sum of the individual effects of pressure and temperature, obtained at ambient temperature and pressure, respectively. The differences between the pressures calculated with the slope determined in this study ($\partial\omega_{1008}/\partial P = 5.48(4)$ cm^{-1}/GPa) and Schmidt et al.[32] ($\partial\omega_{1008}/\partial P = 5.8 \pm 0.1$ cm^{-1}/GPa) increases with pressure and reaches approximately 0.1 GPa at 2 GPa and 0.6 GPa at 10 GPa. The residual standard deviation is reduced from 0.30 to 0.15 GPa by replacing the previous slope with our new value; this is partly attributed to the use of different pressure-determination methods. Thus, the two calibrations do not significantly affect pressure estimates, especially at low-pressure experiments, but the advantage of our calibration is its fine internal consistency with the ruby and gold scales. Since both ruby and gold scales are very extensively used, our spectroscopic zircon scale would provide means to minimize discrepancies between previous results with such pressure scales and experimental data collected under more "difficult" conditions where ruby and gold cannot be stably used as pressure markers.

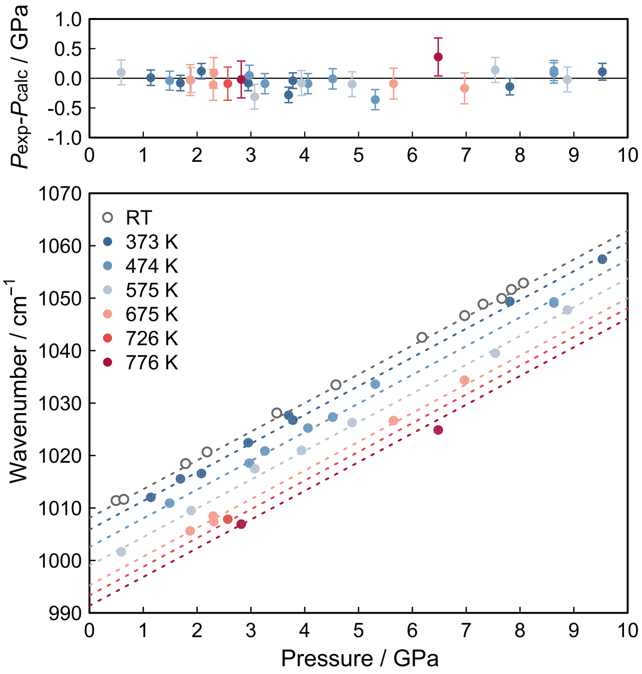

FIGURE 3 Pressure and temperature-dependent B_{1g} mode wavenumber of zircon. Dashed lines are drawn from Equation (5). The top panel shows the difference between the experimental data and calculated values from Equation (6). In the lower panel, the total propagated errors of the random errors and the standard errors of the fitting results fall in the size of the symbol.

Here, we describe the precision of the zircon pressure scale by using the fitting parameters. The estimating error in parameter b in Equations (1), (5), and (6) (5.48 (4) cm^{-1}/GPa) leads to an uncertainty in pressure of ±0.01 GPa. The pressure uncertainty calculated from the errors in the estimating parameters a_0, a_1, a_2, and a_3 in Equations (4), (5), and (6) becomes more significant with increasing temperature and reaches ±0.31 GPa at 773 K and ±0.76 GPa at 1273 K. We confirmed that the temperature and pressure derivative on the wavenumber of the B_{1g}, ω_{1008} mode is negligible under. The measured pressures are well reproduced by the pressures calculated with Equation (6) with a residual standard deviation of 0.15 GPa (Figure 3).

3.5 | Comparison between zircon and *c*-BN

In this section, we experimentally compare the performance of zircon and *c*-BN as Raman spectroscopic pressure scales for studies of geological fluids in hydrothermal DACs at high temperatures and high pressures. Figure 4 compares representative Raman spectra of zircon and *c*-BN placed in the same sample chamber. Raman spectra of zircon and *c*-BN, both stable in a reactive alkaline solution up to 675 K, have no decrease in the intensities and have a similar full width at half maximum (9.0 cm^{-1} for *c*-BN, 7.5 cm^{-1} for zircon) at elevated pressure and temperature. Pressure values at 675 K estimated using our calibration for zircon and Goncharov et al.[27] for *c*-BN fairly agree within the uncertainty, indicating that the zircon scale is properly calibrated. Both scales are therefore applicable, but we would like to emphasize several advantages of the zircon scale. First, as repeatedly mentioned, our zircon scale is highly consistent with the commonly used ruby and gold scales, which helps to minimize gaps with many previous studies. The experimentally calibrated or validated ranges of Equations (5) and (6) in this study are 0–8 GPa at room temperature, 0–9 GPa at 337–573 K, and 0–7 GPa at 637–776 K. Second, the largest advantage of the zircon scale is that the B_{1g} Raman mode has a large pressure dependence ($\partial\omega_i/\partial P$) with a value of 5.5 cm^{-1}/GPa compared with that of the TO modes of *c*-BN (3.4 cm^{-1}/GPa[23–29]). Third, zircon is also advantageous because of its intense

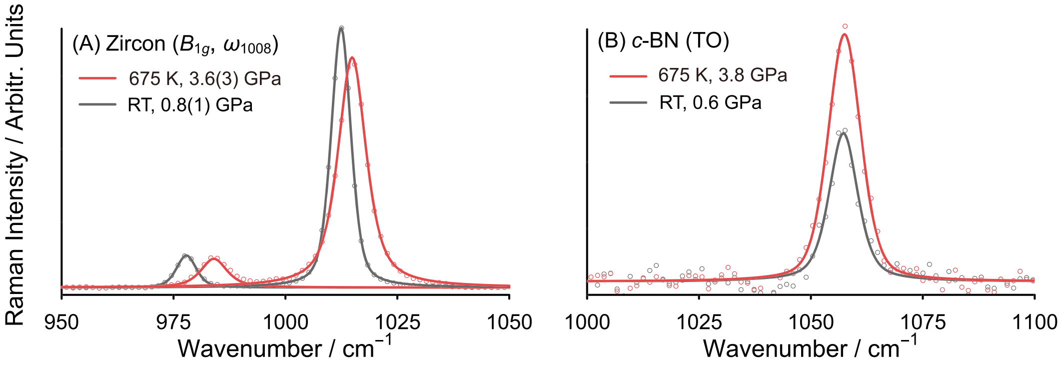

FIGURE 4 Baseline-corrected Raman spectra of zircon and *c*-BN at room temperature and 675 K, with Gaussian–Lorentzian area fitting lines.

Raman peak, giving a better signal-to-noise ratio as shown in Figure 4. Fourth, the scale provides an optional way to precisely determine pressures without spectrometer drift corrections by monitoring the relative wavenumber changes of modes of zircon. Consequently, zircon serves highly accurate and precise pressure estimations at elevated temperatures and pressures.

For future studies, some drawbacks of the zircon scale should also be mentioned. The most problematic fact is that zircon readily decomposes into ZrO_2 and SiO_2 under low silica activity at elevated temperatures.[36] In addition, care should be taken when natural zircon is used instead of synthetic one. This is because natural zircon generally contains Zr-substituting impurities such as U, Th, and Hf, which can cause small down-shifts in the Raman B_{1g}, ω_{1008} mode.[68,69] Radiation damage caused by the radioactive decay of U and Th has also a major influence on the Raman wavenumber at ambient conditions[70–72] and the pressure-induced shifts.[48,50] Since the B_{1g}, ω_{1008} mode at ambient conditions shows moderate down-shifts and band broadening with the accumulation of radioactive decay, the Raman wavenumber and the bandwidth of the mode have been proposed as a method to examine the degree of radiation damage in zircon.[70] These parameters can be criteria for selecting natural zircon as the pressure scale of high-pressure experiments.

4 | CONCLUSIONS

The pressure and temperature dependence of the Raman active modes of synthetic crystalline zircon up to 9.5 GPa and from room temperature to 776 K was investigated using ruby and gold pressure references. The results of the pressure-induced and temperature-induced wavenumber changes for each mode were combined with the existing thermal expansion and compressibility data to evaluate the respective contributions of volume and temperature to the isobaric temperature dependence. The wavenumbers of the B_{1g}, ω_{1008} mode showed excellent linear pressure dependence up to 9.5 GPa along isotherms from 373 to 675 K, which was consistent with the room-temperature coefficient of 5.48(4) cm^{-1}/GPa calculated based on the bivariate weighted method. The individual pressure and temperature effects are independent of each other and are thus also valid under simultaneously elevated temperature and pressure conditions. Our results emphasize that zircon is a reliable and internally consistent Raman-spectroscopy pressure scale for studying geological fluids using DACs at high temperatures and high pressures.

ACKNOWLEDGMENTS

We would like to thank Kazuki Komatsu and Takanori Murakami for their support of experiments. N. Takahashi appreciates Michihiko Nakamura for using the HDAC experimental apparatus and Yuuki Hagiwara for fruitful discussions. Constructive comments from two anonymous reviewers helped to improve the manuscript. The XRD measurements were performed at the BL-18C beamline at the Photon Factory, KEK (proposal numbers: 2020G635 and 2021G663). This research was supported by grants from JSPS KAKENHI JP22J00992 to N. Takahashi. H. Kobayashi acknowledges support from MERIT-WINGS program of the University of Tokyo.

ORCID

Naoko Takahashi https://orcid.org/0000-0002-3518-8934
Hiroki Kobayashi https://orcid.org/0000-0002-3682-7558
Hiroyuki Kagi https://orcid.org/0000-0002-8587-1213

REFERENCES

[1] W. J. Carter, S. P. Marsh, J. N. Fritz, R. G. McQueen, *Natl. Bur. Stand. Spec. Pub.* **1971**, *326*, 147.

[2] C.-S. Zha, H. Mao, R. J. Hemley, *Proc. Natl. Acad. Sci.* **2000**, *97*, 13494.

[3] R. A. Forman, G. J. Piermarini, J. D. Barnett, S. Block, *Science* **1972**, *176*, 284.

[4] H. K. Mao, J. Xu, P. M. Bell, *J. Geophys. Res.* **1986**, *91*, 4673.

[5] K. Syassen, *High Pres. Res.* **2008**, *28*, 75.

[6] D. D. Ragan, R. Gustavsen, D. Schiferl, *J. Appl. Phys.* **1992**, *72*, 5539.

[7] A. Lacam, C. Chateau, *J. Appl. Phys.* **1989**, *66*, 366.

[8] F. Datchi, R. LeToullec, P. Loubeyre, *J. Appl. Phys.* **1997**, *81*, 3333.

[9] S. V. Raju, J. M. Zaug, B. Chen, J. Yan, J. W. Knight, R. Jeanloz, S. M. Clark, *J. Appl. Phys.* **2011**, *110*, 023521.

[10] Q. Jing, Q. Wu, L. Liu, J. Xu, Y. Bi, Y. Liu, H. Chen, S. Liu, Y. Zhang, L. Xiong, Y. Li, J. Liu, *J. Appl. Phys.* **2013**, *113*, 023507.

[11] S. V. Rashchenko, A. Kurnosov, L. Dubrovinsky, K. D. Litasov, *J. Appl. Phys.* **2015**, *117*, 145902.

[12] N. J. Hess, D. Schiferl, *J. Appl. Phys.* **1992**, *71*, 2082.

[13] Y. Zhao, W. Barvosa-Carter, S. D. Theiss, S. Mitha, M. J. Aziz, D. Schiferl, *J. Appl. Phys.* **1998**, *84*, 4049.

[14] A. F. Goncharov, J. M. Zaug, J. C. Crowhurst, E. Gregoryanz, *J. Appl. Phys.* **2005**, *97*, 094917.

[15] Q. Wei, N. Dubrovinskaia, L. Dubrovinsky, *J. Appl. Phys.* **2011**, *110*, 043513.

[16] D. M. Trots, A. Kurnosov, T. B. Ballaran, S. Tkachev, K. Zhuravlev, V. Prakapenka, M. Berkowski, D. J. Frost, *J. Geophys. Res. Solid Earth* **2013**, *118*, 5805.

[17] F. Datchi, P. Loubeyre, R. LeToullec, *Phys. Rev. B* **2000**, *61*, 6535.

[18] F. Datchi, A. Dewaele, P. Loubeyre, R. Letoullec, Y. Le Godec, B. Canny, *High Pres. Res.* **2007**, *27*, 447.

[19] C. Schmidt, M. A. Ziemann, *Am. Mineral.* **2000**, *85*, 1725.

[20] D. Schiferl, M. Nicol, J. M. Zaug, S. K. Sharma, T. F. Cooney, S.-Y. Wang, T. R. Anthony, J. F. Fleischer, *J. Appl. Phys.* **1997**, *82*, 3256.

[21] B. O. Mysen, S. Yamashita, *Geochim. Cosmochim. Acta* **2010**, *74*, 4577.

[22] P. Munsch, H. Bureau, M. E. Yakoubi, H. Khodja, A. Zaitsev, *Eur. J. Mineral.* **2015**, *27*, 365.

[23] T. Kawamoto, K. N. Matsukage, T. Nagai, K. Nishimura, T. Mataki, S. Ochiai, T. Taniguchi, *Rev. Sci. Instrum.* **2004**, *75*, 2451.

[24] F. Datchi, B. Canny, *Phys. Rev. B* **2004**, *69*, 144106.

[25] A. F. Goncharov, J. C. Crowhurst, J. K. Dewhurst, S. Sharma, *Phys. Rev. B* **2005**, *72*, 100104.

[26] F. Datchi, A. Dewaele, Y. L. Godec, P. Loubeyre, *Phys. Rev. B* **2007**, *75*, 214104.

[27] A. F. Goncharov, J. C. Crowhurst, J. K. Dewhurst, S. Sharma, C. Sanloup, E. Gregoryanz, N. Guignot, M. Mezouar, *Phys. Rev. B* **2007**, *75*, 224114.

[28] S. Ono, K. Mibe, N. Hirao, Y. Ohishi, *J. Phys. Chem. Solid* **2015**, *76*, 120.

[29] L. Ren, C. Wang, X. Li, R. Tao, *Am. Mineral.* **2023**, *108*, 455.

[30] A. Watenphul, C. Schmidt, *J. Raman Spectrosc.* **2012**, *43*, 564.

[31] K. K. Zhuravlev, A. F. Goncharov, S. N. Tkachev, P. Dera, V. B. Prakapenka, *J. Appl. Phys.* **2013**, *113*, 113503.

[32] C. Schmidt, M. Steele-MacInnis, A. Watenphul, M. Wilke, *Am. Mineral.* **2013**, *98*, 643.

[33] S. Farsang, S. Facq, S. A. T. Redfern, *Am. Mineral.* **1988**, *2018*, 103.

[34] C. Schmidt, I.-M. Chou, *Eur. Mineral. U. Notes Mineral.* **2012**, *12*, 249.

[35] M. Wilke, C. Schmidt, J. Dubrail, K. Appel, M. Borchert, K. Kvashnina, C. E. Manning, *Earth Planet. Sci. Lett.* **2012**, *349–350*, 15.

[36] D. Bernini, A. Audétat, D. Dolejš, H. Keppler, *Geochim. Cosmochim. Acta* **2013**, *119*, 178.

[37] E. B. Watson, T. M. Harrison, *Earth Planet. Sci. Lett.* **1983**, *64*, 295.

[38] E. B. Watson, D. J. Chemiak, J. M. Hanchar, T. M. Harrison, D. A. Wark, *Chem. Geol.* **1997**, *141*, 19.

[39] J. M. Hanchar, R. J. Finch, P. W. O. Hoskin, E. B. Watson, D. J. Cherniak, A. N. Mariano, *Am. Mineral.* **2001**, *86*, 667.

[40] S. Ono, K. Funakoshi, Y. Nakajima, Y. Tange, T. Katsura, *Contrib. Mineral. Petrol.* **2004**, *147*, 505.

[41] C. Stangarone, R. J. Angel, M. Prencipe, B. Mihailova, M. Alvaro, *Am. Mineral.* **2019**, *104*, 830.

[42] P. Dawson, M. M. Hargreave, G. R. Wilkinson, *J. Phys. C: Solid State Phys.* **1971**, *4*, 240.

[43] R. W. G. Syme, D. J. Lockwood, H. J. Kerr, *J. Phys. C: Solid State Phys.* **1977**, *10*, 1335.

[44] N. Sheremetyeva, D. J. Cherniak, E. B. Watson, V. Meunier, *Phys. Chem. Miner.* **2018**, *45*(2), 173.

[45] B. A. Kolesov, C. A. Geiger, T. Armbruster, *Eur. J. Mineral.* **2001**, *13*, 939.

[46] L. Nasdala, M. Zhang, U. Kempe, G. Panczer, M. Gaft, M. Andrut, M. Plötze, *Rev. Mineral. Geochem.* **2003**, *53*, 427.

[47] C. Stangarone, R. J. Angel, M. Prencipe, N. Campomenosi, B. Mihailova, M. Alvaro, *Eur. J. Mineral.* **2019**, *31*, 685.

[48] L. Nasdala, R. Miletich, K. Ruschel, T. Váczi, *Phys. Chem. Miner.* **2008**, *35*, 597.

[49] E. Knittle, Q. Williams, *Am. Mineral.* **1993**, *78*, 245.

[50] F. A. Pina Binvignat, T. Malcherek, R. J. Angel, C. Paulmann, J. Schlüter, B. Mihailova, *Phys. Chem. Miner.* **2018**, *45*, 981.

[51] P. I. Dorogokupets, A. R. Oganov, *Phys. Rev. B* **2007**, *75*, 024115.

[52] P. I. Dorogokupets, A. Dewaele, *High Pres. Res.* **2007**, *27*, 431.

[53] W. A. Bassett, A. H. Shen, M. Bucknum, I. Chou, *Rev. Sci. Instrum.* **1993**, *64*, 2340.

[54] A. J. Anderson, P. Meredith, W. A. Bassett, R. Mayanovic, C. Benmore, Proceedings of the CNS 2nd Canada-China Joint Workshop on SuperCritical Water-Cooled Reactors (SCWR), **2010**.

[55] G. J. Piermarini, S. Block, J. D. Barnett, *J. Appl. Phys.* **1973**, *44*, 5377.

[56] R. J. Angel, M. Bujak, J. Zhao, G. D. Gatta, S. D. Jacobsen, *J. Appl. Cryst.* **2007**, *40*, 26.

[57] S. Klotz, J.-C. Chervin, P. Munsch, G. Le Marchand, *J. Phys. D Appl. Phys.* **2009**, *42*, 075413.

[58] R. L. McCreery, *Raman spectroscopy for chemical analysis*, John Wiley & Sons, New York **2000**, 157.

[59] S. Fukura, T. Mizukami, S. Odake, H. Kagi, *Appl. Spectrosc.* **2006**, *60*, 946.

[60] G. J. Piermarini, S. Block, J. D. Barnett, R. A. Forman, *J. Appl. Phys.* **1975**, *46*, 2774.

[61] Y. Seto, D. Nishio-Hamane, T. Nagai, N. Sata, *Rev. High Press. Sci. Technol.* **2010**, *20*, 269.

[62] A. C. Larson, R. B. V. Dreele, *Report IAUR* **1994**, *86*, 475.
[63] B. H. Toby, *J. Appl. Cryst.* **2001**, *34*, 210.
[64] D. York, N. M. Evensen, M. L. Martínez, J. De Basabe Delgado, *Am. J. Physiol.* **2004**, *72*, 367.
[65] K. Thirumalai, A. Singh, R. Ramesh, *J. Geol. Soc. India* **2011**, *77*, 377.
[66] B. A. Weinstein, R. Zallen, in *Topics Appl. Phys. 54 light scattering in solids IV*, (Eds: M. Cardona, G. Güntherodt), Springer, Berlin Heidelberg **1984**, 463.
[67] A. M. Ehlers, G. Zaffiro, R. J. Angel, T. Boffa-Ballaran, M. A. Carpenter, M. Alvaro, N. L. Ross, *Am. Mineral.* **2022**, *107*, 74.
[68] T. Geisler, B. E. Burakov, V. Zirlin, L. Nikolaeva, P. Pöml, *Eur. J. Mineral.* **2005**, *17*, 883.
[69] N. Sheremetyeva, D. J. Cherniak, E. B. Watson, V. Meunier, J. Condens, *Matter Phys.* **2019**, *31*, 455402.
[70] L. Nasdala, G. Irmer, D. Wolf, *Eur. J. Mineral.* **1995**, *7*, 471.
[71] M. Zhang, E. K. H. Salje, I. Farnan, A. Graeme-Barber, P. Daniel, R. C. Ewing, A. M. Clark, H. Leroux, *J. Phys. Condens. Matter* **1915**, *2000*, 12.
[72] N. Campomenosi, D. Rubatto, J. Hermann, B. Mihailova, M. Scambelluri, M. Alvaro, *Am. Mineral.* **2020**, *105*, 992.

SUPPORTING INFORMATION

Additional supporting information can be found online in the Supporting Information section at the end of this article.

How to cite this article: N. Takahashi, H. Kobayashi, H. Kagi, *J Raman Spectrosc* **2024**, *55*(6), 706. https://doi.org/10.1002/jrs.6663